Supporting Information

Design and oxidative desulfurization of Ag/Ti heterometallic clusters based on Hard−Soft Acid−Base principle

Shuyi Yang,[a] Yaomei Fu,[b] Yiran Tian,[a] Liang Zhao,*[ac] , Xinlong Wang*[a] and Baoli Li*[ac]

[a] Key Laboratory of Polyoxometalate and Reticular Material Chemistry of Ministry of Education, Northeast Normal University, Changchun, 130024, China

E-mail: zhaol352@nenu.edu.cn, wangxl824@nenu.edu.cn

[b] Shandong Peninsula Engineering Research Center of Comprehensive Brine Utilization, Weifang University of Science and Technology, Shouguang, 262700, China

[c] Changchun Baoli Science and Technology Co. Changchun, 130024, China

1. Crystallographic details

Table S1 The Crystallographic data for $\mathbf{Ag_2Ti_{10}}$, $\mathbf{Ag_2Ti_{11}}$ (CCDC: **2277822-2277823**)

Compound	$\mathbf{Ag_2Ti_{10}}$	$\mathbf{Ag_2Ti_{11}}$
Empirical formula	$C_{158}H_{140}Ag_2N_4O_{62}Ti_{10}$	$C_{116}H_{116}Ag_2O_{64}Ti_{11}$
Formula weight	3781.47	3276.72
Crystal system	Monoclinic	Monoclinic
Space group	$P2_1/c$	$C2/c$
Temperature (K)	173.02	173.02
Wavelength (Å)	0.71073 A	0.71073A
a (Å)	19.1273(9)	21.292(5)
b (Å)	23.1405(10)	39.754(9)
c (Å)	37.5489(16)	16.628(4)
α (°)	90	90
β (°)	95.0750(10)	92.036(8)
γ (°)	90	90
Volume (Å^3)	16554.6(13)	14066(6)
Z	4	4
$D_{calc.}$ /g·cm^{-3}	1.518	1.547
μ/mm-1	0.776	0.952
F(000)	7710.0	6640.0
Limiting indices	$-22 \le h \le 22$, $-27 \le k \le 27$, $-41 \le l \le 44$	$-25 \le h \le 25$, $-47 \le k \le 47$, $-18 \le l \le 19$
Theta range for data collection (°)	4.424 to 50.116	4.902 to 50.124
Reflections collected	117523	67489
Independent reflections	28882 [R(int) = 0.1568, R(sigma) = 0.1515]	12423 [R(int) = 0.1440, R(sigma) = 0.0933]
Refinement method	Full-matrix least-squares on F^2	Full-matrix least-squares on F^2
Data / restraints / parameters	28882/1822/2246	12423/1072/905
Goodness-of-fit on F^2	1.031	1.027
Final R indices [$I > 2$sigma(I)]	$R_1 = 0.0846$, $wR_2 = 0.1734$	$R_1 = 0.0596$, $wR_2 = 0.1357$
R indices (all data)	$R_1 = 0.1990$, $wR_2 = 0.2394$	$R_1 = 0.1168$, $wR_2 = 0.1581$

Table S2 The Crystallographic data for **Ag_2Ti_2** and **Ag_2Ti_{12}** (CCDC: **2277824-2277825**)

Compound	**Ag_2Ti_2**	**Ag_2Ti_{12}**
Empirical formula	$C_{140}H_{120}Ag_4O_{36}P_4Ti_4$	$C_{120}H_{145}Ag_2N_3O_{42}P_2Ti_{12}$
Formula weight	3125.326	3153.86
Crystal system	Triclinic	Monoclinic
Space group	*P*-1	$P2_1/n$
Temperature (K)	173.15	173.02
Wavelength (Å)	0.71073 A	0.71073 A
a (Å)	12.4087(19)	19.6923(16)
b (Å)	14.508(3)	25.691(2)
c (Å)	20.709(4)	30.026(2)
α (°)	103.505(9)	90
β (°)	101.189(8)	108.457(2)
γ (°)	101.414(8)	90
Volume ($Å^3$)	3438.6(11)	14409(2)
Z	1	4
$D_{calc.}$ /g·cm^{-3}	1.509	1.454
μ/mm-1	0.901	0.987
F(000)	1583.0	6440.0
Limiting indices	$-14 \le h \le 14$, $-17 \le k \le 17$, $-24 \le l \le 24$	$-23 \le h \le 23$, $-30 \le k \le 30$, $-32 \le l \le 35$
Theta range for data collection (°)	5.12 to 50.16	4.364 to 50.34
Reflections collected	50748	91182
Independent reflections	12042 [*R*(int) = 0.0560, *R*(sigma) = 0.0462]	25592 [*R*(int) = 0.1225, *R*(sigma) = 0.1305]
Refinement method	Full-matrix least-squares on F^2	Full-matrix least-squares on F^2
Data / restraints / parameters	12042/24/903	25592/488/1395
Goodness-of-fit on F^2	1.067	1.024
Final *R* indices [*I* > 2sigma(I)]	$R_1 = 0.0554$, $wR_2 = 0.1272$	$R_1 = 0.1149$, $wR_2 = 0.2950$
R indices (all data)	$R_1 = 0.0968$, $wR_2 = 0.1702$	$R_1 = 0.2311$, $wR_2 = 0.3970$

2. Powder X-ray diffraction

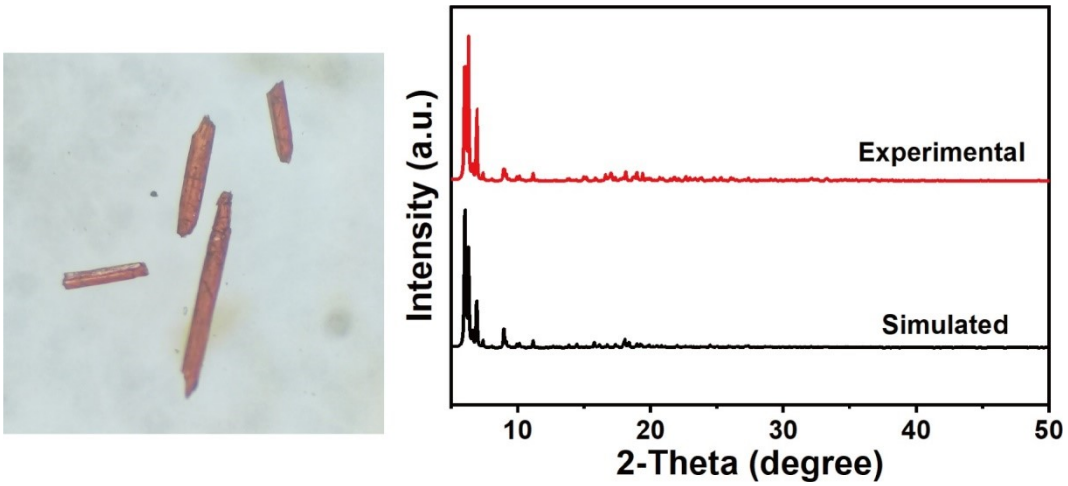

Fig. S1 Optical photograph of Ag_2Ti_{10} crystal (left), and comparision of simulated and experimental PXRD patterns of Ag_2Ti_{10} (right).

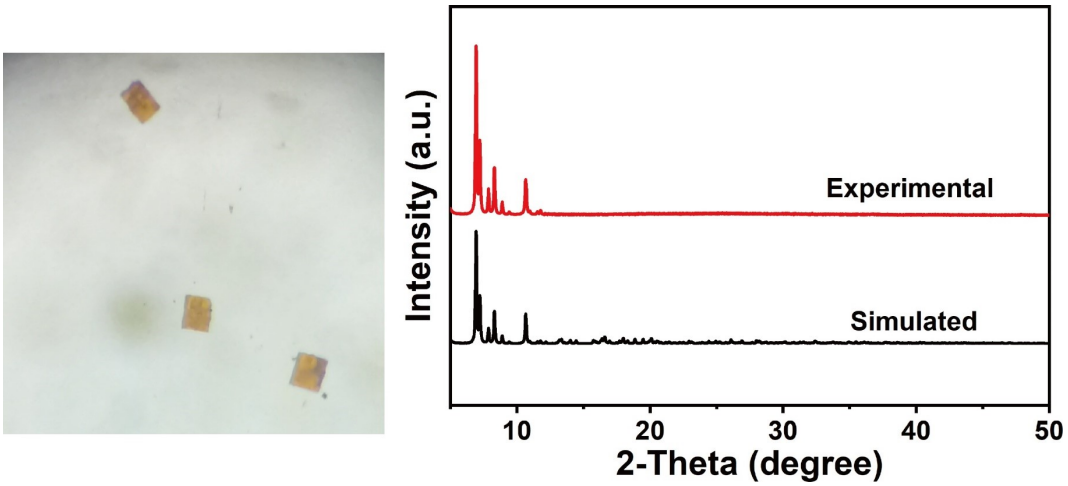

Fig. S2 Optical photograph of Ag_2Ti_{11} crystal (left), and comparision of simulated and experimental PXRD patterns of Ag_2Ti_{11} (right).

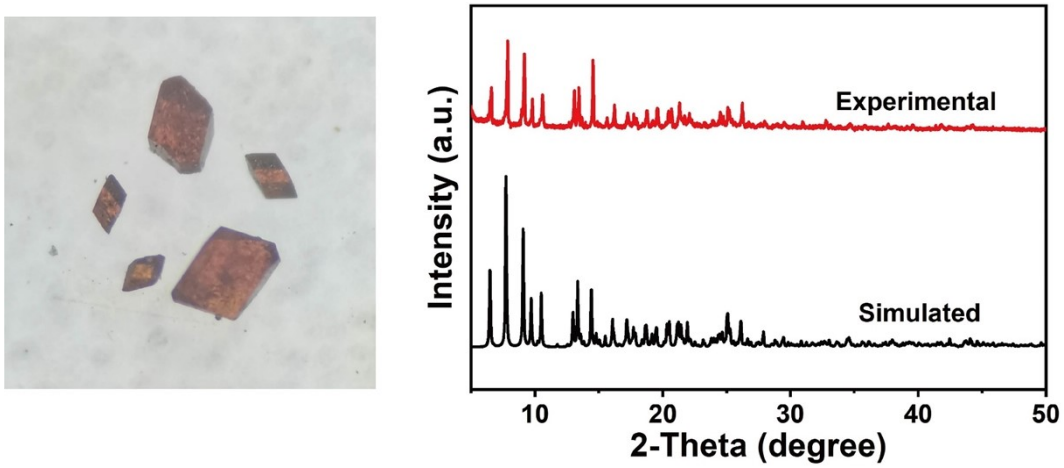

Fig. S3 Optical photograph of Ag_2Ti_2 crystal (left), and comparision of simulated and experimental PXRD patterns of Ag_2Ti_2 (right).

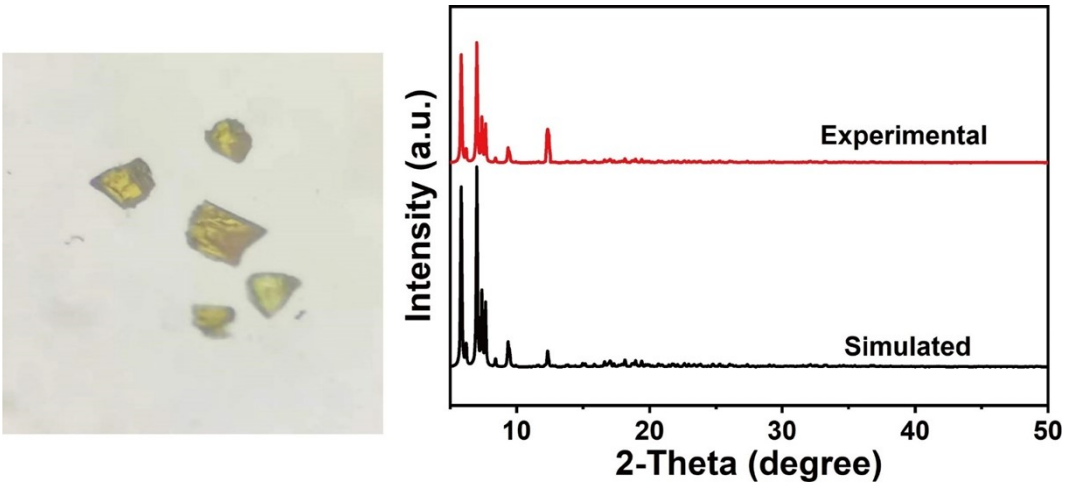

Fig. S4 Optical photograph of Ag_2Ti_{12} crystal (left), and comparision of simulated and experimental PXRD patterns of Ag_2Ti_{12} (right).

3. TG-Measurement

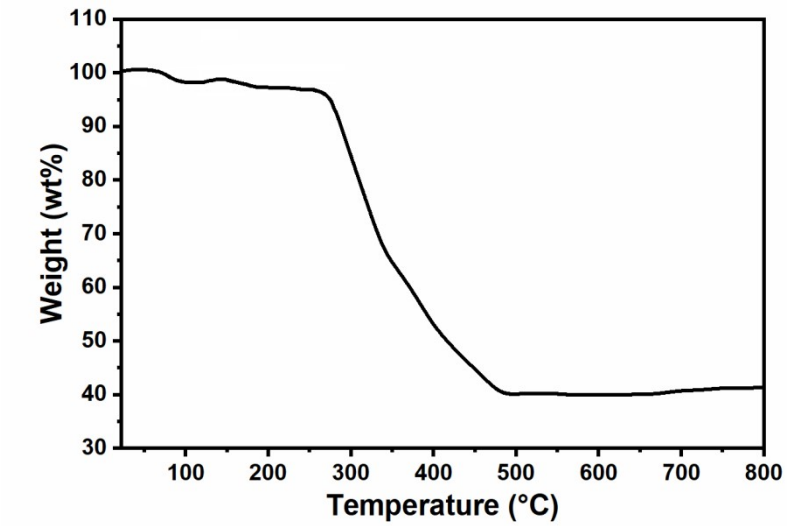

Fig. S5 TG curve of Ag_2Ti_{10}.

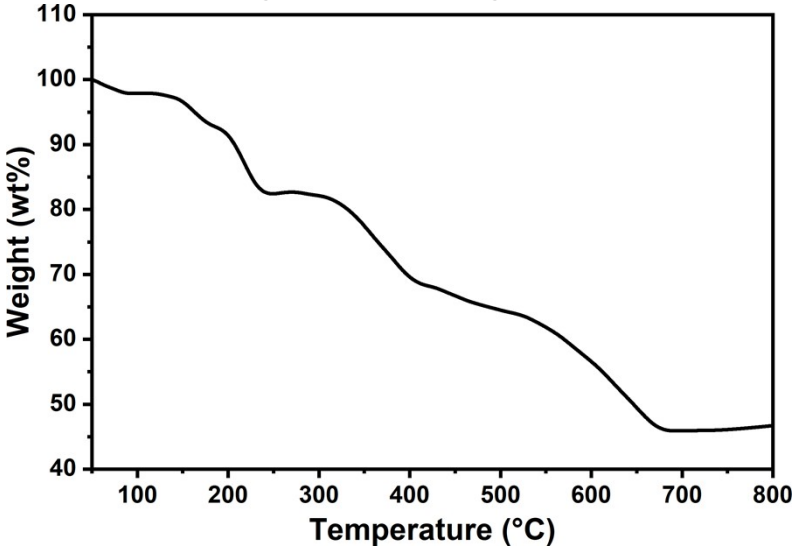

Fig. S6 TG curve of Ag_2Ti_{11}

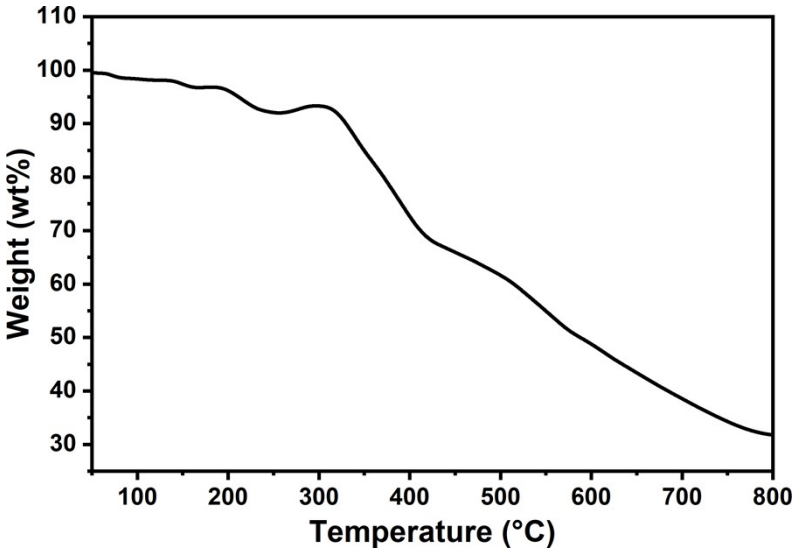

Fig. S7 TG curve of Ag_2Ti_2

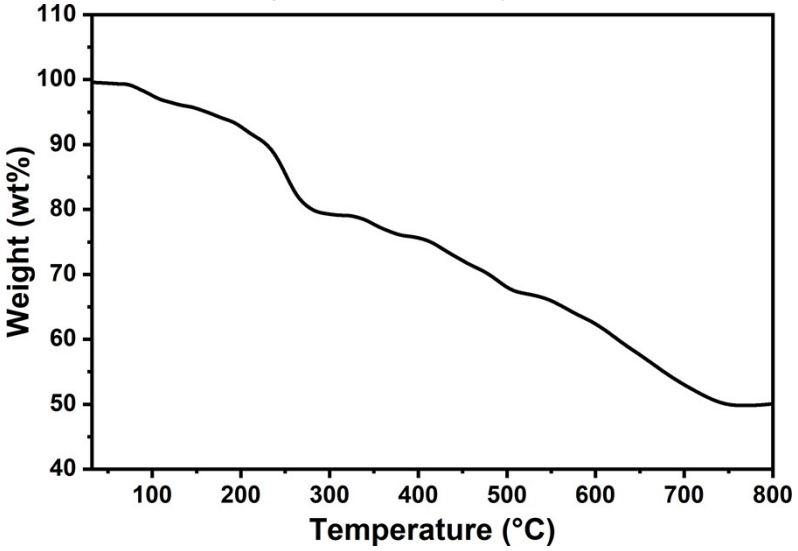

Fig. S8 TG curve of Ag_2Ti_{12}

4. FT-IR spectra

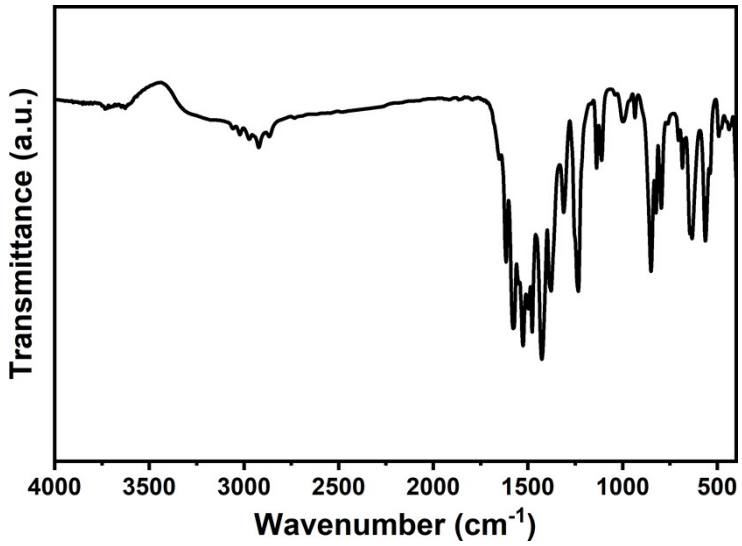

Fig. S9 FT-IR spectrum of Ag_2Ti_{10}

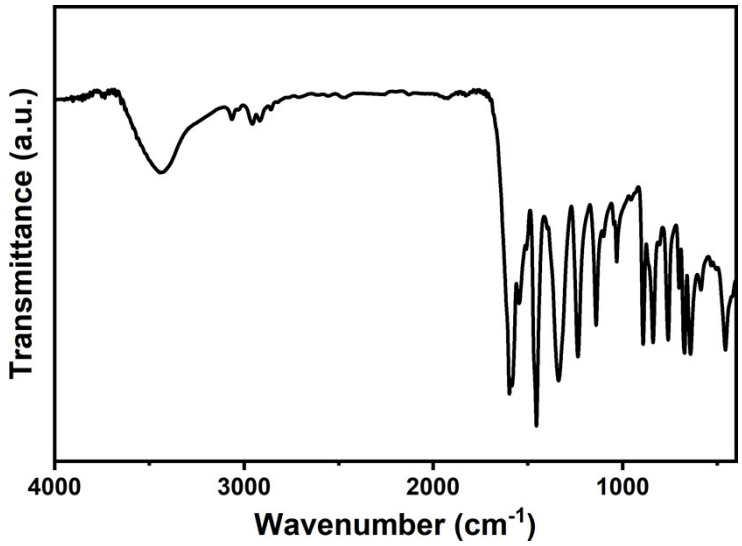

Fig. S10 FT-IR spectrum of $\mathbf{Ag_2Ti_{11}}$

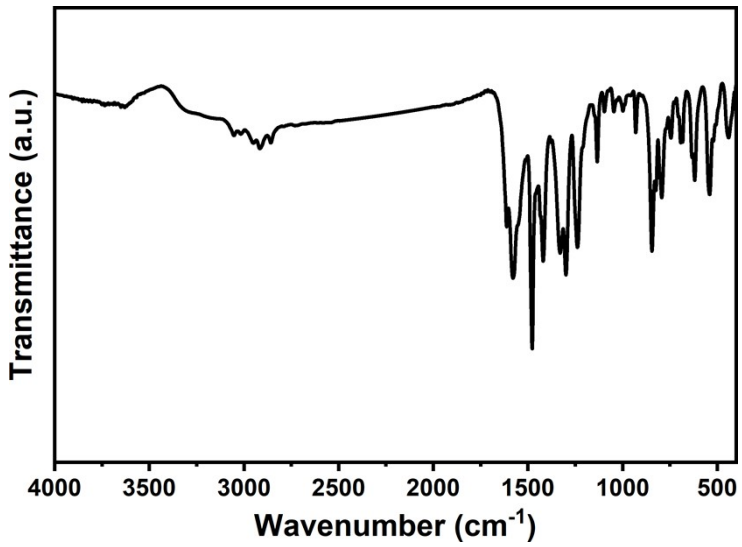

Fig. S11 FT-IR spectrum of $\mathbf{Ag_2Ti_2}$

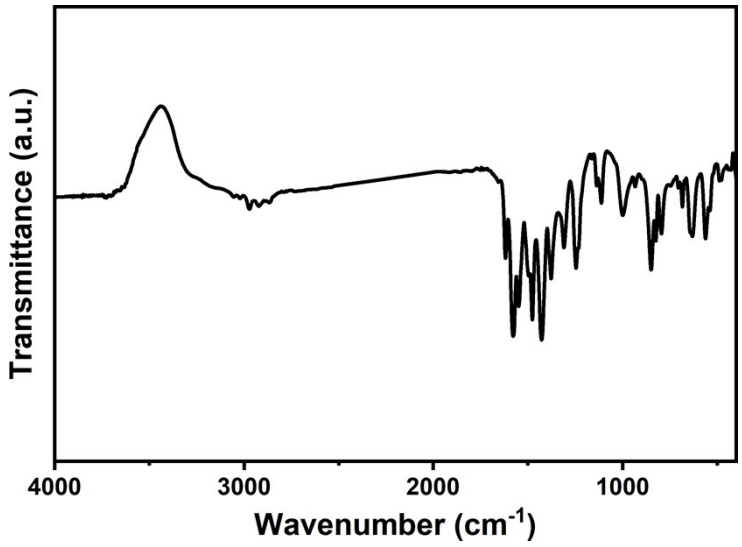

Fig. S12 FT-IR spectrum of $\mathbf{Ag_2Ti_{12}}$

5. Solid UV–vis adsorption spectra

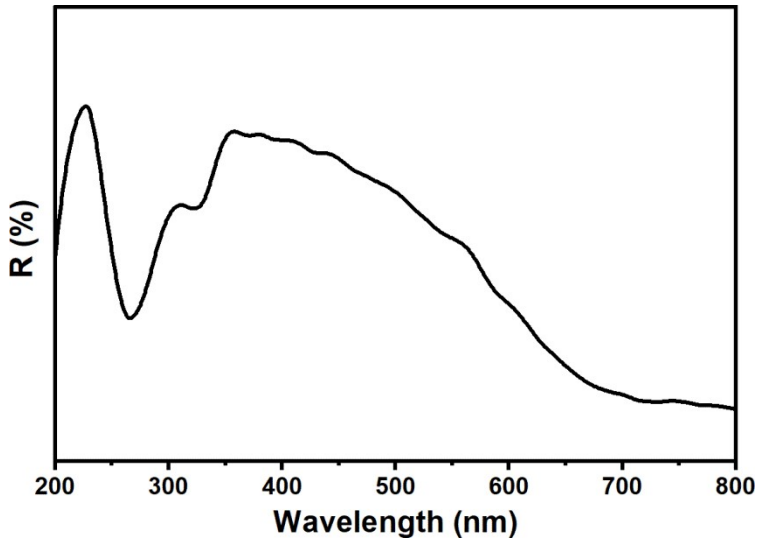

Fig. S13 Solid UV–vis adsorption spectrum of Ag_2Ti_{10}

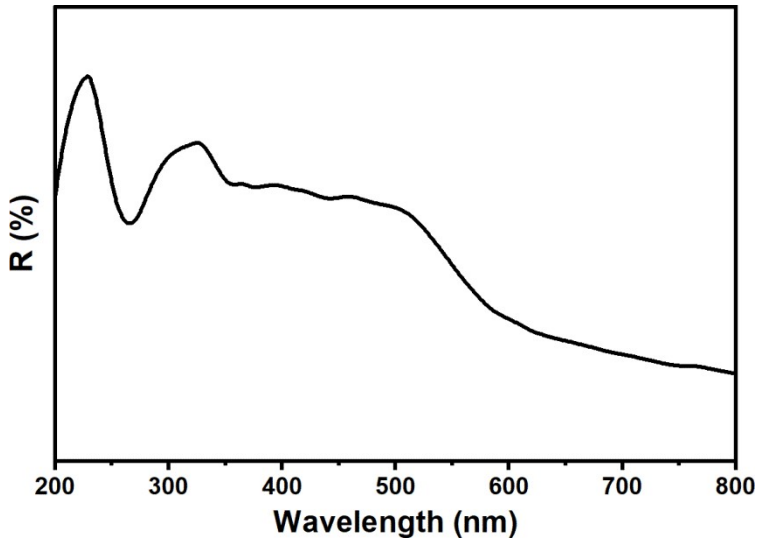

Fig. S14 Solid UV–vis adsorption spectrum of Ag_2Ti_{11}

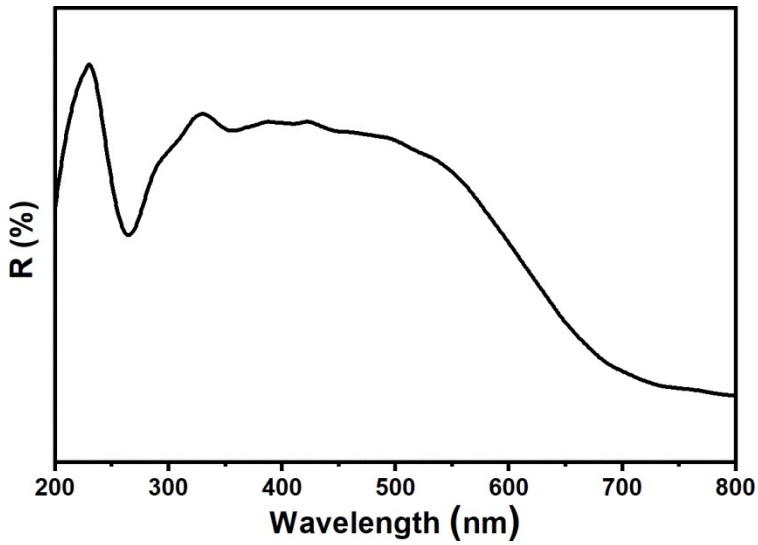

Fig. S15 Solid UV–vis adsorption spectrum of Ag_2Ti_2

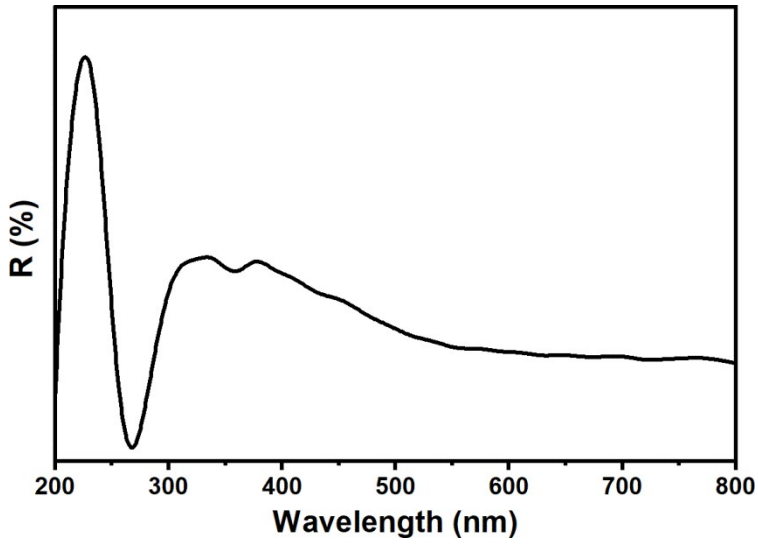

Fig. S16 Solid UV–vis adsorption spectrum of Ag_2Ti_{12}

6. Structure of the clusters

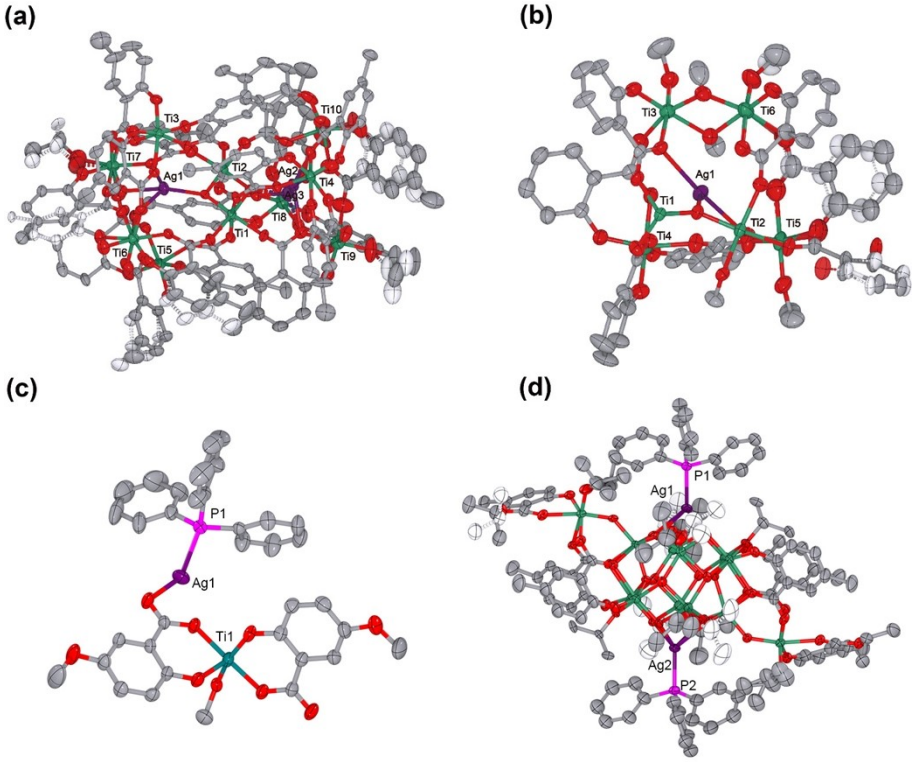

Fig. S17 Thermal ellipsoid plot drawings of the crystal structures of compounds **1-4**.

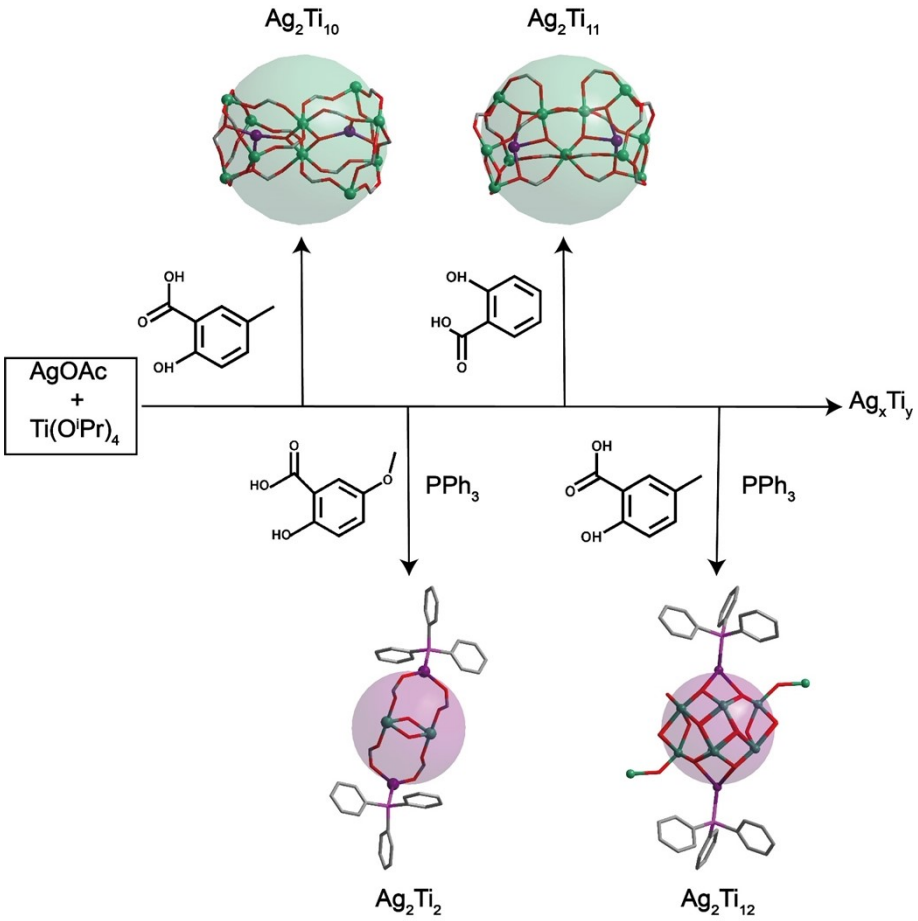

Scheme S1 Schematic synthesis of four heterometallic Ag/Ti clusters.

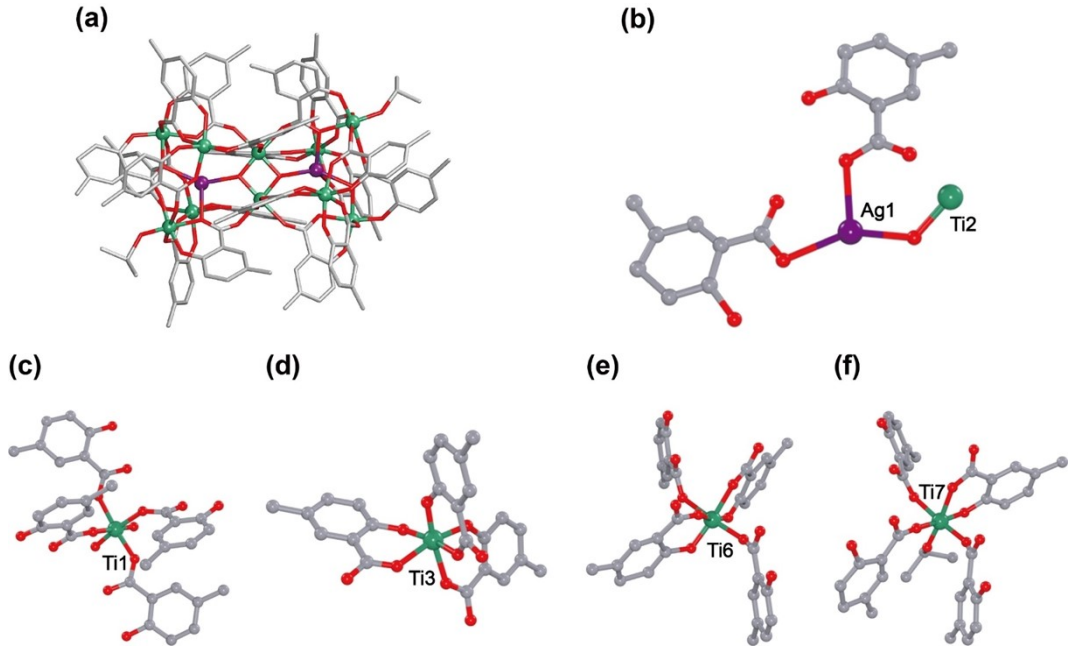

Fig. S18 (a) Molecular structure of $\mathbf{Ag_2Ti_{10}}$. (b-f) Coordination environments of **Ag1**, **Ti1**, **Ti3**, **Ti6** and **Ti7** in $\mathbf{Ag_2Ti_{10}}$.

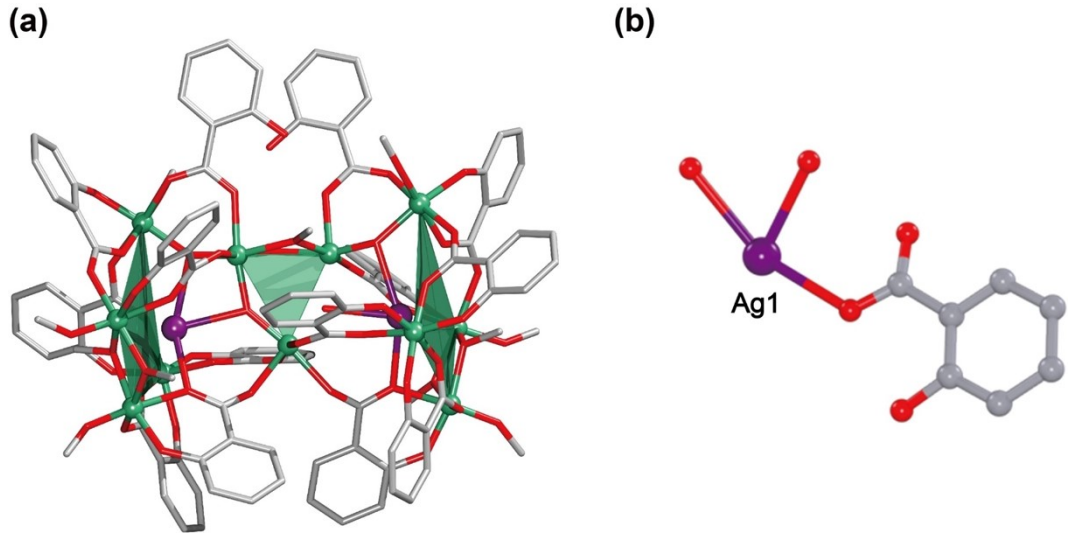

Fig. S19 (a) Molecular structure of $\mathbf{Ag_2Ti_{11}}$. (b) Coordination environments of Ag atom in $\mathbf{Ag_2Ti_{11}}$.

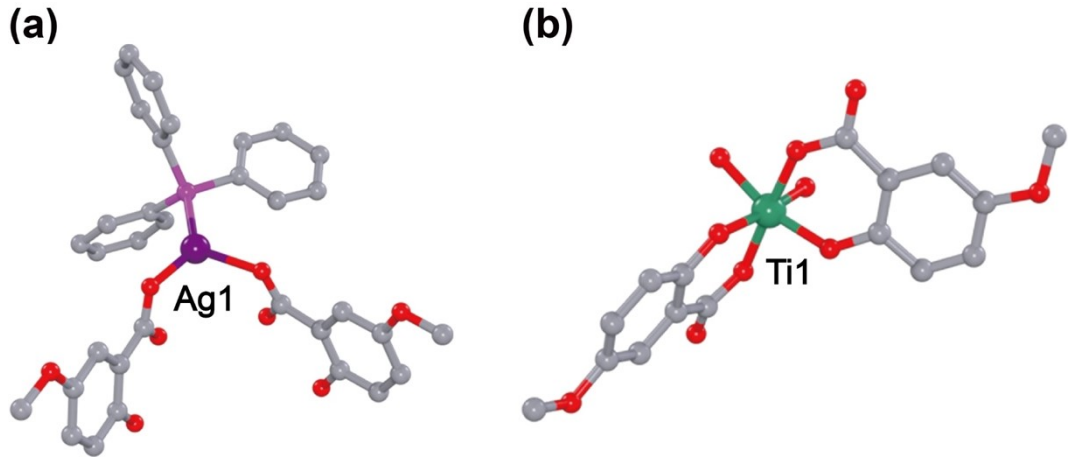

Fig. S20 Coordination environments of Ag atom (a) and Ti atom (b) in $\mathbf{Ag_2Ti_2}$.

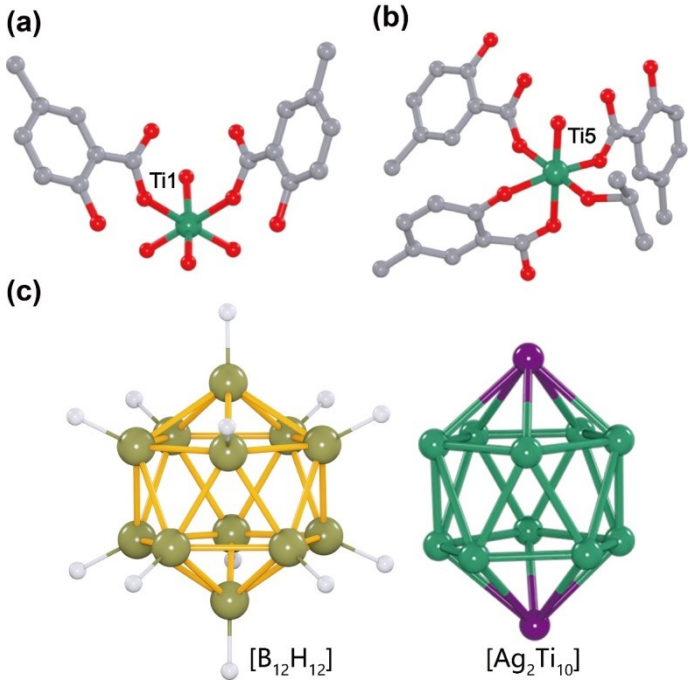

Fig. S21 (a) and (b) Two coordination environments of Ti atoms in $\mathbf{Ag_2Ti_{12}}$. (c) Representation of the conformations of

$[B_{12}H_{12}]$ and $[Ag_2Ti_{10}]$ core in **Ag_2Ti_{12}**.

7. Desulfurization test characterization

Table S3 The control experiments for selective oxidation of thioanisole to methyl phenyl sulfoxide by different catalysts.

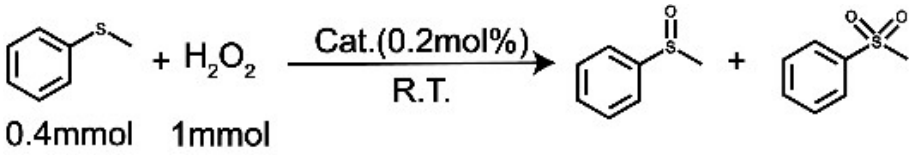

Entry	Catalyst	Temp.(℃)	Time	Conv.(%)
1	AgOAc	r.t.	30 min	0
2	$Ti(O^iPr)_4$	r.t.	30 min	0
3	Mixture	r.t.	30 min	74.03
4	Ag_2Ti_{10}	r.t.	30 min	98.21
5	Ag_2Ti_{11}	r.t.	30 min	97.82
6	Ag_2Ti_2	r.t.	30 min	96.34
7	Ag_2Ti_{12}	r.t.	30 min	99.96

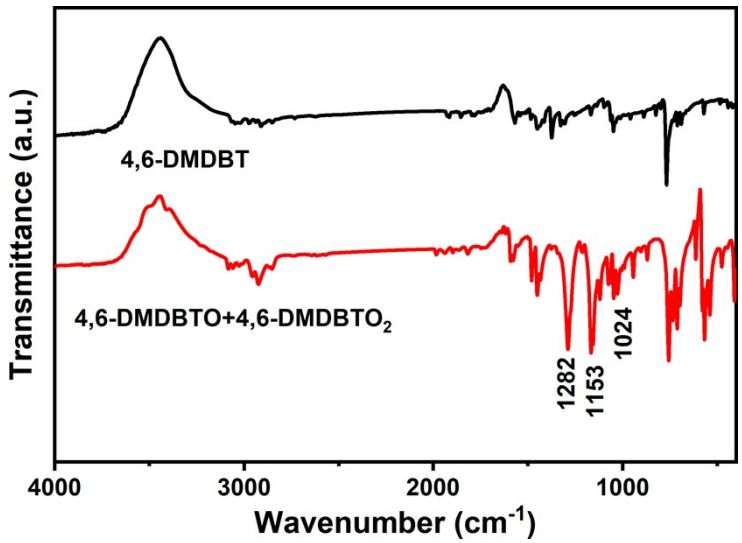

Fig. S22 FT-IR spectra of the 4,6-DMDBT (black) and the corresponding catalytic oxidation products of the 4,6-DMDBTO and 4,6-DMDBTO 2 (red). The characteristic frequencies at ν_{as} (O=S=O) = 1282 cm^{-1}, ν_{as} (O=S=O) = 1153 cm^{-1} and ν(S=O) = 1024 cm^{-1} suggest the appearance of the sulfoxides and sulfones.

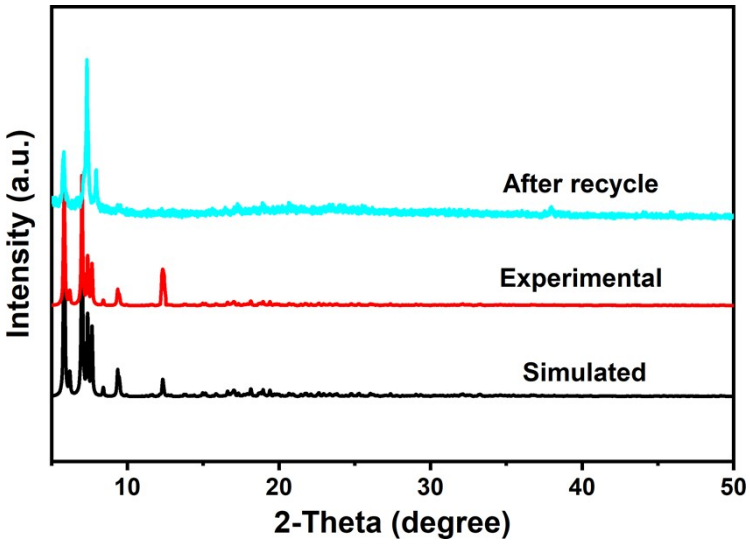

Fig. S23 The PXRD patterns for Ag_2Ti_{12}: Simulated (black), Experimental (red), After recycle (light blue).

Table S4 Controlled experiments of catalytic oxidation of DBT or MBT reported in the literature

Entry	Sulfide	Catalyst	Temp.(℃)	Oxidant	Time(min)	Conv.(%)	Ref.
1	MBT	$CuCl_2$	40	TBHP	240	28	1
2	MBT	$NiCl_2 \cdot 6H_2O$, TMR4A	50	TBHP	60	25	2
3	MBT	[a]$[Co_2L_{0.5}V_4O_{12}]\cdot 3DMF\cdot 5H_2O$	50	TBHP	240	99	3
4	MBT	[b]$[Ag_4(PMo_{12}O_{40})(L)_2]\cdot OH$	40	TBHP	240	99	4
5	MBT	[c]P_2W_{15}-γAl_2O_3	25	H_2O_2	35	99	5
6	**MBT**	**1**	**25**	**H_2O_2**	**30**	**98.21**	**This work**
7	**MBT**	**2**	**25**	**H_2O_2**	**30**	**97.82**	**This work**
8	**MBT**	**3**	**25**	**H_2O_2**	**30**	**96.34**	**This work**
9	**MBT**	**4**	**25**	**H_2O_2**	**30**	**99.96**	**This work**
10	DBT	$[Mo_8O_{26}]^{4-}$	30	H_2O_2	90	82.3	6
11	DBT	MoO_3	100	O_2	360	0	7
12	DBT	MoO_3 +CeO_2	100	O_2	360	26	7
13	DBT	[d]$[Co(HBBTZ)(BBTZ)_{2.5}][PMo_{12}O_{40}]$	50	TBHP	540	98.1	8
14	DBT	[e]$[Co(BBPTZ)_3][HPMo_{12}O_{40}]\cdot 24H_2O$	50	TBHP	480	99.16	8
15	DBT	HSiW/h-BN	40	H_2O_2	60	100	9

16	**DBT**	**4**	**50**	**H_2O_2**	**360**	**77.46**	**This work**

[a]L=2-(2-pyridyl)imidazole functionalized resorcin[4]arene; [b]L= sulfur-bridged thiacalix[4]arene; [c]P_2W_{15}= $Na_{12}[\alpha$-$P_2W_{15}O_{56}]\cdot 24H_2O$; [d]BBTZ=4,4′-bis(1,2,4-triazol-1-ylmethyl)benzene; [e]BBPTZ=4,4′-bis(1,2,4-triazol-1-ylmethyl)biphenyl.

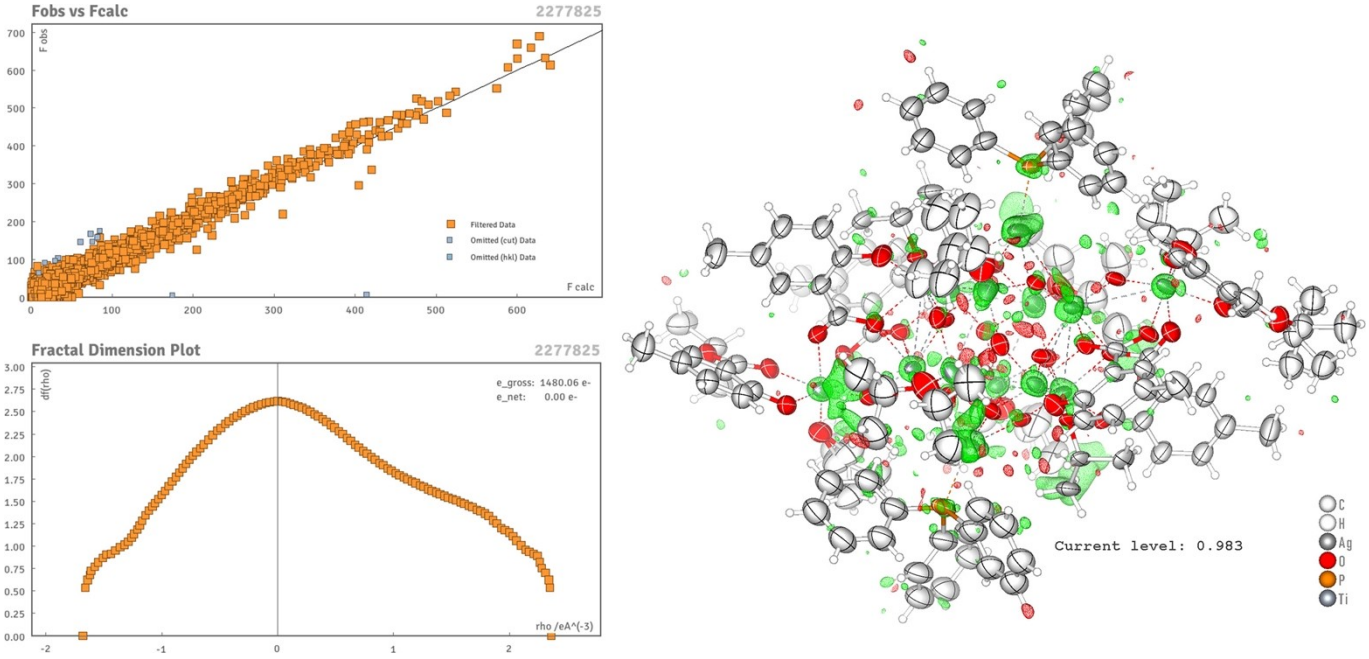

Fig. S24 Fobs vs Fcalc graph and fractal dimension plot for Ag_2Ti_{12} indicate poor data quality (left), the residual density maps obtained for Ag_2Ti_{12} with the contour level was set to 0.983 e $Å^{-3}$. These data show that the current model does not fit the data very well because of the poor diffraction data of Ag_2Ti_{12}.

1 An H, Hou Y, Wang L, et al. Evans−Showell-Type Polyoxometalates Constructing High-Dimensional Inorganic−Organic Hybrid Compounds with Copper−Organic Coordination Complexes: Synthesis and Oxidation Catalysis. *Inorg Chem.*, 2017, **56**, 11619-11632.

2 Yu M Y, Yang J, Xu X, et al. Highly stable polyoxometalate-resorcin[4]arene-based inorganic-organic complexes for catalytic oxidation desulfurization. *Appl Organomet Chem.*, 2019, **33**, e5169.

3 Lu B B, Yang J, Liu Y Y, et al. A Polyoxovanadate–Resorcin[4]arene-Based Porous Metal–Organic Framework as an Efficient Multifunctional Catalyst for the Cycloaddition of CO_2 with Epoxides and the Selective Oxidation of Sulfides. *Inorg Chem.*, 2017, **56**, 11710-11720.

4 Yu M Y, Guo T T, Shi X C, et al. Polyoxometalate-Bridged Cu(I)- andAg(I)-Thiacalix[4]arene Dimers for Heterogeneous Catalytic Oxidative Desulfurization and Azide−Alkyne “Click” Reaction. *Inorg Chem.*, 2019, **58**, 11010-11019.

5 Hong L, Win P, Zhang X, et al. Covalent Immobilization of Polyoxotungstate on Alumina and Its Catalytic Generation of Sulfoxides. *Chem Eur J.*, 2016, **22**, 11232-11238.

6 Yang H, Jiang B, Sun Y, et al. Heterogeneous oxidative desulfurization of diesel fuel catalyzed by mesoporous polyoxometallate-based polymeric hybrid. *J Hazard Mater.*, 2017, **333**, 63-72.

7 Shi Y, Liu G, Zhang B, et al. Oxidation of refractory sulfur compounds with molecular oxygen over a Ce–Mo–O catalyst. *Green Chem.*, 2016, **18**, 5273-5279.

8 Hao X L, Ma Y Y, Zang H Y, et al. A Polyoxometalate-Encapsulating Cationic Metal–Organic Framework as a Heterogeneous Catalyst for Desulfurization. *Chem Eur J.*, 2015, **21**, 3778-3784.

9 Ji H, Sun J, Wu P, et al. Silicotungstic acid immobilized on lamellar hexagonal boron nitride for oxidative desulfurization of fuel components. *Fuel.*, 2018, **213**, 12-21.